Visualization and analysis of structural ordering during crystallization of a gold nanoparticle

Yu Hang Chui, Ian K. Snook, and Salvy P. Russo*
Applied Physics, School of Applied Sciences, RMIT University, G.P.O. Box 2476V, Melbourne, Victoria 3001, Australia
(Received 7 January 2007; revised manuscript received 2 August 2007; published 16 November 2007)

In this molecular dynamics study, we provide an insight into the crystallization of a liquid droplet by following the structural ordering of the surface and core atoms in a 10 179 atom gold nanoparticle quenched from the melt down to 298 K. We use the $Q6$ order parameter and ring statistics to measure the degree of crystallization during quenching and a topological structure measure based on planar graphs to visualize the time evolution of structural ordering of the nanoparticle core at the temperature where significant crystallization first occurs (949 K). Our results indicate that crystallization of the surface precedes that of the core and, in fact, provides a template for the ordering of the core region. There is also evidence presented that hcp twin planes form directly below the region where the edges of two (111) surface planes meet. At 298 K, the nanoparticle forms a defected icosahedral structure, and we observe the formation of fcc fragments and hcp planes characteristic of an icosahedral structure in the core as a function of temperature.

DOI: 10.1103/PhysRevB.76.195427 PACS number(s): 61.46.Df

I. INTRODUCTION

Crystallization is of enormous importance both from a fundamental and from an applied perspective. The theory of crystallization from a dense disordered system has been shown to be inadequately described by classical nucleation theory, and so the mechanism of crystallization is still an open question. From a practical point of view, crystallization is of vital importance in growing materials with useful properties which have a wide range of applications. Thus, understanding crystallization is vital to the controlled production of useful materials.

The importance of crystallization is nowhere more apparent than in nanoparticle production and utilization. For example, gold nanoparticles have been shown to be the most promising nanomaterial with a wide range of potential applications in electronics, biomedicine, optics, and catalysis.[1] Critical parameters that affect the electronic, optical, and catalytic properties of these nanoparticles are their size and shape.[2–6] Therefore, understanding the mechanisms underlying the crystallization of these particular nanoparticles is important if one hopes to control their size and morphology and therefore their properties. The simplest process for growing nanogold is by vapor condensation in an inert atmosphere at low pressure. High resolution transmission electron microscopy analysis of gold nanoparticles grown by vapor condensation due to quenching in helium at low pressure shows that the icosahedral (Ih) morphology is the dominant morphology for particles smaller than 12 nm, followed by decahedral and fcc.[7]

Theoretical studies of the crystallization of small gold nanoparticles ($<$1000 atoms) have revealed two important points regarding their growth: (1) the Ih morphology constitute a local minima in the cluster free energy[8] and (2) crystallization appears to initiate from the surface and proceed into the cluster core.[9–11]

However, the detailed crystallization dynamics of large gold nanoparticles ($>$3 nm) is still unknown. Koga *et al.*[7] comment that the relatively large abundance of particles of Ih morphology over other morphologies in a size range corresponding to several nanometers cannot be understood by only considering energetics. Therefore, here, we study the kinetics of the crystallization process of a 10 179 atom ($\sim$8 nm in diameter) icosahedral gold nanoparticle which is quenched from the melt by a combination of molecular dynamics (MD) simulation and analysis of the local structure using a topological method based on planar graphs.[10,12,13] Using this topological analysis method, we can determine whether the local packing of the nanocluster core is fcc, hcp, defected fcc, or defected hcp and follow the growth or rearrangement of fcc fragments and hcp planes in the core as a function of temperature.

II. METHOD

A. Computational details

The embedded atom "glue" potential was used to model the atomic interactions, as this potential has been shown to effectively reproduce the bulk, surface, and defect properties of gold.[14] The quenched icosahedral clusters were produced by melting perfect icosahedral clusters, which were generated by an icosahedron generation program,[15] to 1400 K. Once in the liquid state, the liquid gold clusters were quenched from 1400 to 1000 K using a cooling rate of 2×10^{-11} s/K and from 1000 to 298 K with a cooling rate of 1×10^{-10} s/K. At each temperature studied in this work, we followed the time evolution of crystallization by MD out to 0.4 ns. The MD time step was 5 fs.

B. Structure analysis

An often used geometric measure for crystallization is the $Q6$ order parameter which measures the orientational order of an atomic system[12,13] and may be used as a convenient order parameter to follow crystallization but gives little detailed information about structural evolution. Thus, in addition, we use planar graph analysis[10] to give detailed analysis of local ordering. A planar graph representation of the local environment about a particular atom is the two dimensional projection of the three dimensional nearest neighbor connec-

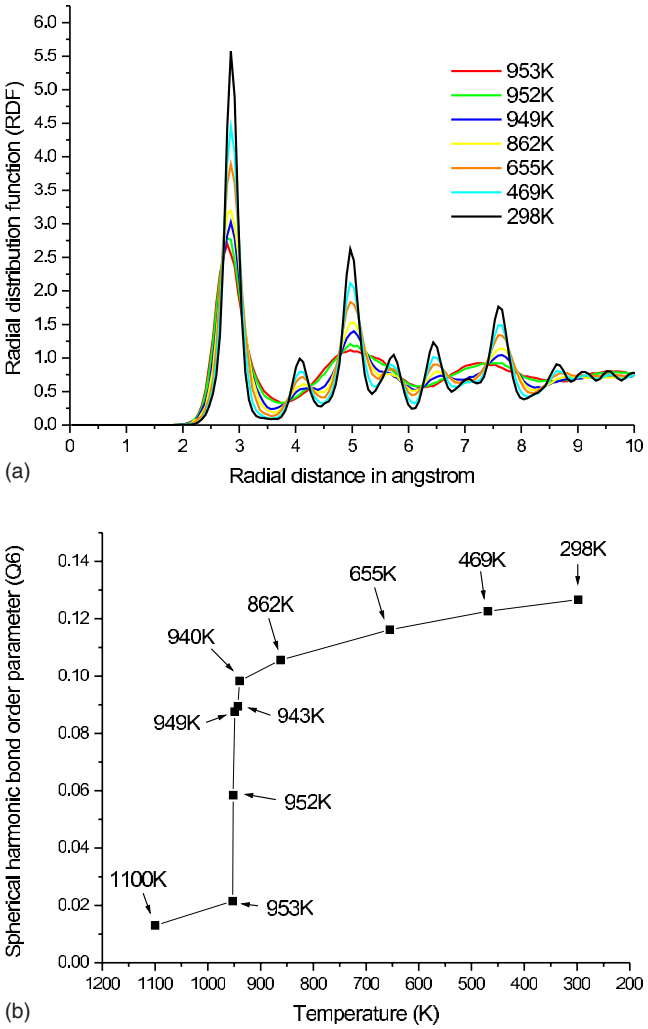

FIG. 1. (Color online) (a) The variation of the radial distribution function of a Au 10 179 nanoparticle during the quenching process. (b) The variation of bond order parameter ($Q6$) during the quenching of a Au 10 179 nanoparticle. The sharp rise of $Q6$ indicates that the rapid crystallization occurs between 952 and 940 K.

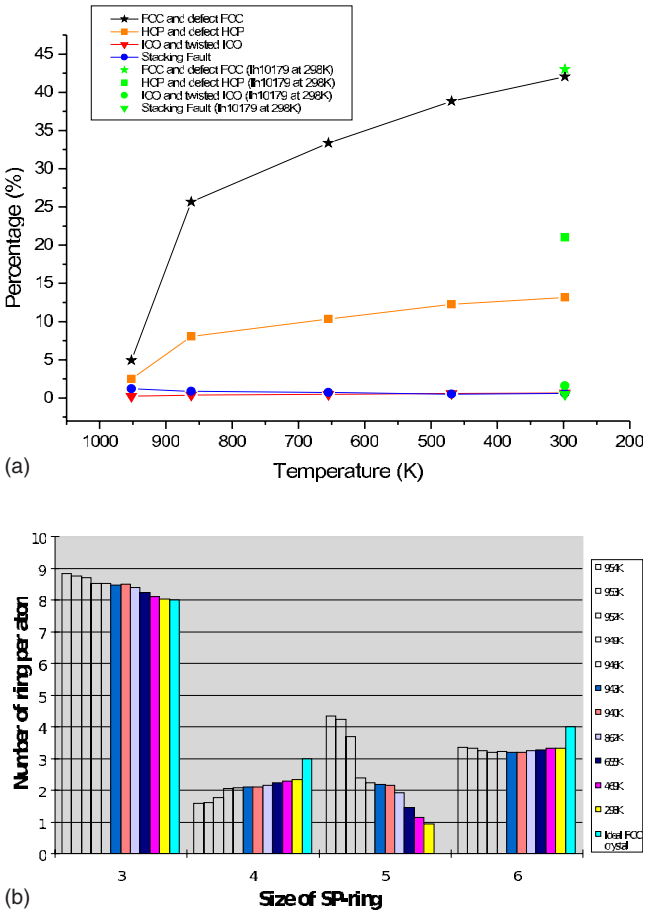

FIG. 2. (Color online) (a) The percentage variation of fcc, hcp, ICO, and stacking fault content in a Au 10 179 nanoparticle during the quench. Green symbols indicate the structural contents of a perfect icosahedron at 298 K. (b) The statistics of shortest-path (SP) ring of a Au 10 179 gold nanocluster during the quenching process.

tions to that atom. In the planar graph representation, atoms are represented as a set of vertices, joined by lines (bonds) between nearest neighbors such that no two lines cross one another. In this method, two particles are regarded as being bonded if their distance is less than or equal to the first minimum of the radial distribution function. Hence, bonds are defined geometrically rather than chemically.

By characterizing the number and structure of rings of various sizes making up the planar graph, we can classify the local environment about an atom.[10,16] In this work, we classified the local environment by considering only the number of different sized rings about an atom.

Another measure of structure is given by ring statistics. In this work, the shortest-path (SP) ring structure criterion due to Fransblau[17] is used, which defines a ring as the SP ring if the number of bonds passed through in moving from one particle of the ring to another is equal to the shortest path, considering all possible paths through the network of bonds from one particle to another. The "distance" between two particles is defined as the minimum number of bonds that would have to be traversed in order to move from one particle to another. The distance which is not the physical bond length is 1 for nearest neighbors, 2 for next nearest neighbors, and so on. Using the SP ring criterion, the simplest quantities obtainable from ring analysis are the ring statistics, that is, the prevalence of the ring types observed. The term "ring size" refers to the number of molecules in the ring and not the physical dimension.[13] The SP ring structures evaluated here range in ring size from 3 to 6.

This method has proven to be useful in finding the structural characteristics in common (and not in common) for ordered and disordered systems. Further details regarding SP ring statistics are given in Ref. 18.

III. RESULTS

A. Crystallization during quenching

A commonly used structure measure is the radial distribution function (RDF), and the change in the RDF of a gold nanocluster during quenching from 1100 to 298 K is shown in Fig. 1(a). Figure 1(a) definitely shows that structural or-

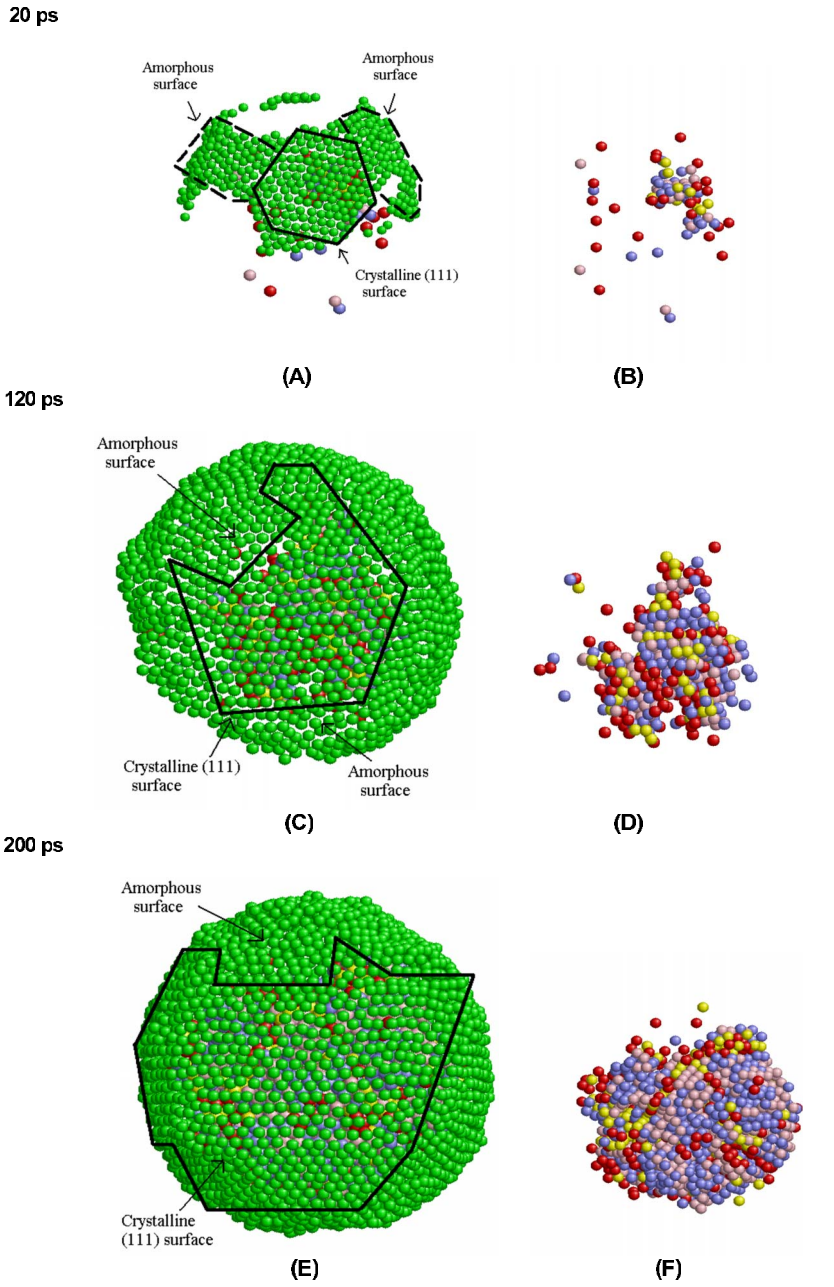

FIG. 3. (Color online) [(a) and (b)] The correlation between structural ordering occurring in the surface and core atoms after 20 ps at 949 K; [(c) and (d)] and [(e) and (f)] are after 120 and 200 ps, respectively. The following color scheme is used to classify the core atoms: fcc (pink), defected fcc (blue), hcp (yellow), and defected hcp (red). Note that the ordered core region occurs directly below the ordered surface regions which, however, form first.

dering is occurring as the temperature is decreased; however, it is too coarse a measure to give a precise estimation of the freezing temperature, but this can be clearly observed from the behavior of the $Q6$ order parameter which was calculated after running an MD simulation for 0.4 ns at each particular temperature, as shown in Fig. 1(b). The sharp transition in $Q6$ gives a clear indication of the significant structural ordering occurring between 952 and 940 K, which suggests that the freezing temperature occurs in this range, which is not evident from the RDF.

In order to give a quantitative determination of how the internal structure of the nanocluster core is evolving, we now show the relative percentage of the atoms in an fcc, hcp, and icosahedral (ICO) environments [Fig. 2(a)] and shortest-path ring statistics [Fig. 2(b)], over the same temperature range. Figure 2(a) indicates that structure of the gold nanocluster moves toward that of a perfect icosahedron [whose characteristics are shown as green symbols in Fig. 2(b)] as temperature is decreased but shows that some disorder still exists in the final, kinetically grown crystal. In particular, in Fig. 2(b), the average number of five membered rings in the core gives an indication of structural disorder, as this number is zero in a bulk defect-free environment, and in this figure, this number uniformly deceases from 4.34 to 0.93 with the sharpest drop occurring between 952 and 949 K, which is consistent with the freezing temperature being in this range as indicated by the $Q6$ data [Fig. 1(b)].

B. Mechanism of crystallization of a Au nanoparticle

As stated in the Introduction, one of the fundamental, unanswered questions in condensed matter physics and materials science is "what is the mechanism of crystallization?" Classical nucleation theory essentially says that when a

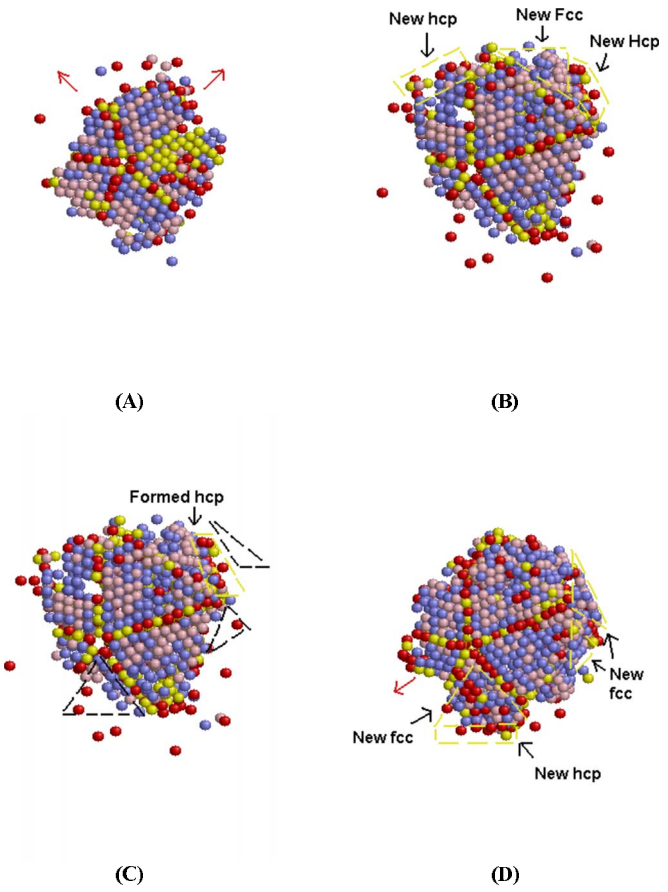

FIG. 4. (Color online) Snapshots in the time evolution of the core at (a) 160 ps, [(b) and (c)] 180 ps, and (d) 200 ps. The direction in which crystallization occurs is indicated by red arrows. Yellow and dotted black lines represent the regions where we believe fcc fragments or hcp planes are beginning to form.

metastable disordered region of an inhomogeneous system reaches a certain critical size, then the gain in free energy due to this bulklike region will exceed the free energy penalty due to the creation of its surface and the region will grow and a new phase will appear. However, this description does not describe the mechanism for the formation of a crystal, and the equations resulting from this theory do not give an adequate description of nucleation and growth of crystals, particularly colloidal crystals. Thus, one can say that this theory only gives an energy based criterion for the stability and growth or decay of a new, dense region, but it does not describe a mechanism for the appearance of crystalline order in a disordered system. Nanodrops are an excellent system in which to study this mechanism as essentially a high density disordered phase can be produced whose structural evolution can be followed both theoretically and experimentally. Recent simulation and experimental studies of a nanodrop in a vacuum suggest that crystallization occurs first at the surface and then occurs in the bulk.[9–11] However, it is still unclear if this is definitely so and if it is what is the relationship between the surface and core ordering processes, i.e., do they occur independently or do they depend on one another in some way? In order to help answer this question, we have directly observed this structural ordering process and have

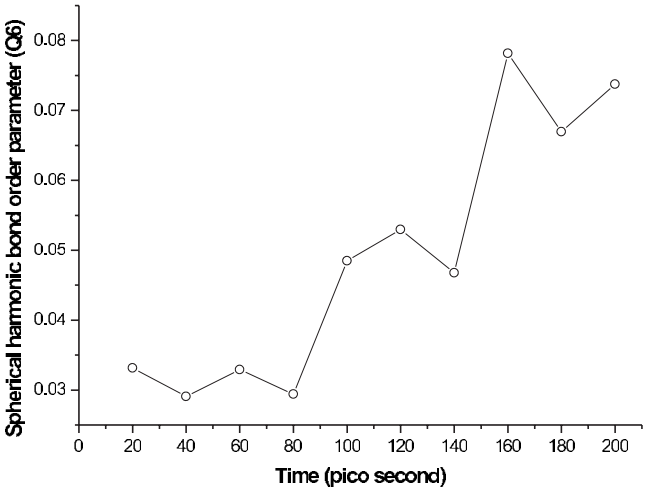

FIG. 5. The variation of bond order parameter ($Q6$) during the first 200 ps of crystallization of a Au 10 179 nanoparticle at 949 K.

analyzed the surface ordering by following the evolution of the (111) planes and of the nanoparticle core by use of our planar graph method to characterize the local bonding structure of the core atoms. Furthermore, in order to demonstrate the high level of order achieved in this process, we also compare our structural analysis of a recrystallized particle with that of a perfect icosahedron. We classify the local environment about each core gold atom using the following color scheme: fcc (pink), defected fcc (blue), hcp (yellow), and defected hcp (red).

Figures 3 and 4 show snapshots of a typical gold nanoparticle at various time sequences during the evolution of the crystallization process at 949 K, which is a temperature at which large scale ordering is occurring based on Figs. 1 and 2.

The diagrams shown in Fig. 3 should be viewed as pairs, the first of which, e.g., Fig. 3(a), shows the surface structure in the region where ordering is occurring and the second, e.g., Fig. 3(b), shows any ordering occurring in the core at the same time. Also, the relationship between these two regions is shown in the first of each paired figure as the core atoms which are ordered can be seen behind the surface atoms (shown in green).

Firstly, Fig. 3(a) shows that the surface starts to order into some clearly visible (111) surface regions after quite a short time (20 ps at 949 K), while the paired Fig. 3(b) shows that at the same time, no significant ordering occurs in the core. It should be noted that atoms not shown in the core are not of a highly ordered type.

At some time later (120 ps), Fig. 3(c) shows that although the surface structure has not evolved significantly, the core has now started to order noticeably and that the ordered region is directly below the initially ordered surface region as shown by the increased ordering of the core atoms (seen through the green colored ordered surface atoms in the figure). Figure 3(d) is effectively Fig. 3(c) with the surface atoms removed to give a clearer visualization of the core. Figures 3(e) and 3(f) show the status of the surface and core regions after 200 ps at 949 K. These figures strongly indicate that the (111) region formed at early times on the surface has

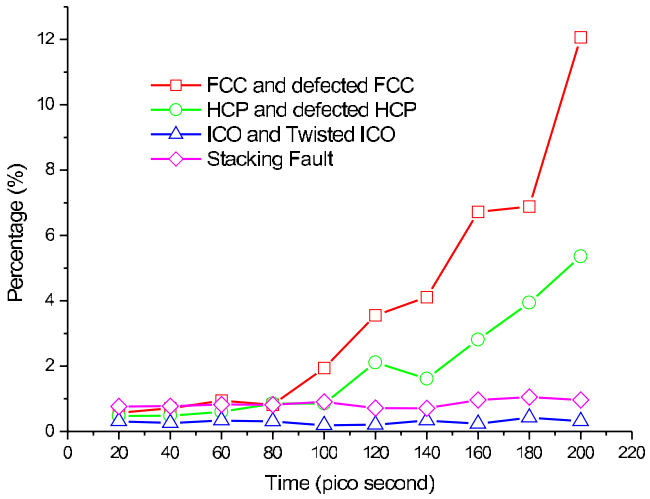

FIG. 6. (Color online) The percentage variation of fcc, hcp, ico, and stacking fault content in a Au 10 179 nanoparticle during the first 200 ps of crystallization at 949 K.

acted as a template for the ordering of the core.

Figure 4 shows snapshots in the time evolution of the core at 949 K corresponding to 160 ps (a), 180 ps [(b) and (c)], and 200 ps (d). In Fig. 4(a) (160 ps), we indicate the direction in which crystallization is preceded by red arrows, and 20 ps later [Fig. 4(b)], we observe that the atoms in the regions indicated by these arrows have transformed from a disordered state to one where the local environment is fcc or

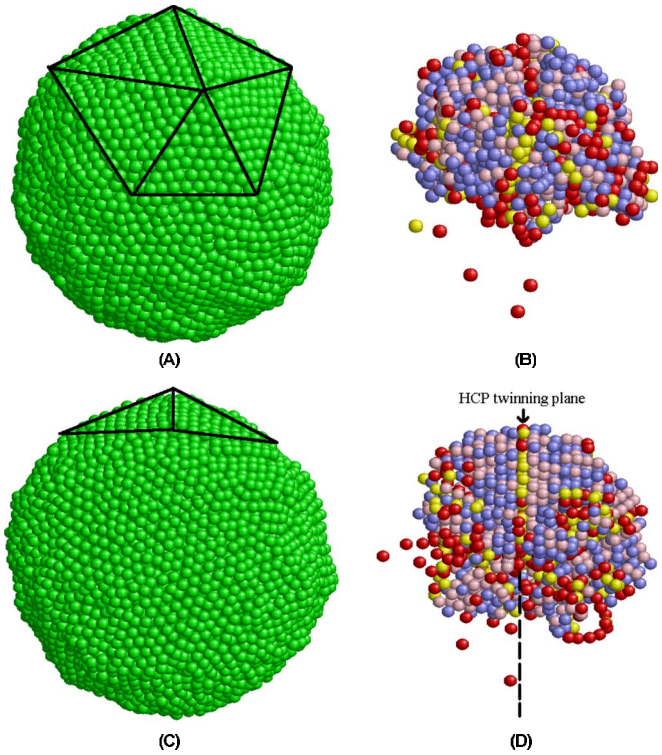

FIG. 7. (Color online) The surface and core structure of the Au nanoparticle after 200 ps from two different visual perspectives. For the surface atoms, the black triangles indicate sections of (111) planes. The formation of a twin plane is shown in (d).

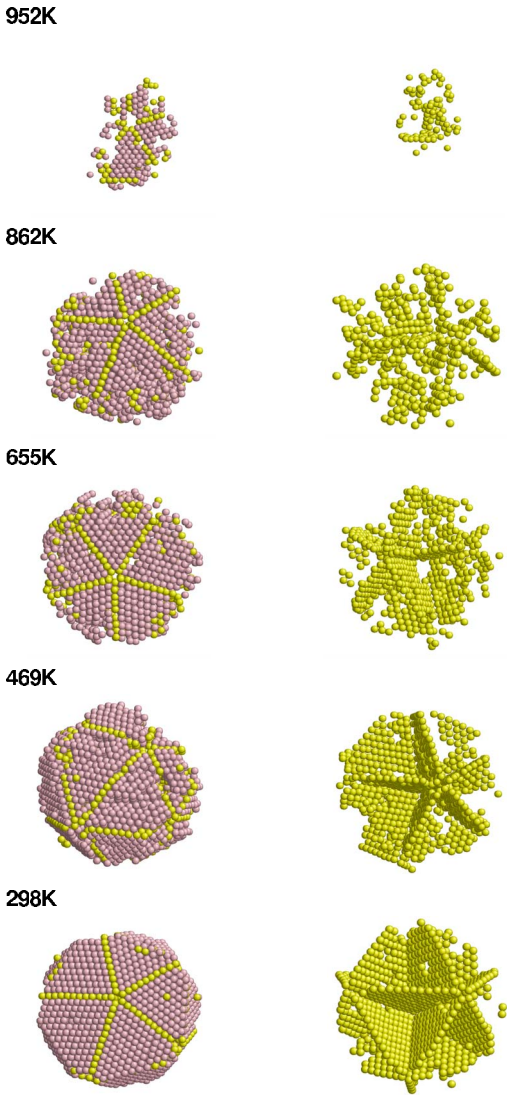

FIG. 8. (Color online) The temperature evolution of the core atoms from 952 to 298 K in a Au 10 179 nanoparticle. fcc fragments and hcp planes are shown on the left and the evolution of the hcp plane network on the right.

hcp. In Fig. 4(b), we indicate (using yellow dotted lines) the regions where we believe fcc fragments or hcp planes are beginning to form. In Fig. 4(c) (180 ps), we again indicate, using black dotted lines, regions where newly formed fcc fragments have formed at 200 ps [Fig. 4(d)].

To quantify the time evolution of the structural crystallization which we have shown visually in the preceding figures occurring at 949 K, we show how the $Q6$ order parameter (Fig. 5) and the relative percentage of the core atoms in an fcc, hcp, and ICO environments (Fig. 6) change from 20 to 200 ps. Figures 5 and 6 show that crystallization of the nanocluster begins approximately after 80 ps at 949 K. Figure 6 also indicates that in the crystallization process, blocks of fcc form before the formation of hcp planes. We note that the value of the $Q6$ parameter at 949 K in Fig. 2 is higher than that in Fig. 5 because in Fig. 2, $Q6$ was calculated, at each temperature, after running MD for 0.4 ns, whereas in Fig. 5, $Q6$ is given from 20 to 200 ps.

To further emphasize the key role played by the surface in inducing crystallization in the core region, we show the initial formation of a twin plane in the core of the gold nanoparticle after 200 ps in the time evolution. Figure 7 shows the surface and core structure after 200 ps but from two different visual perspectives. For the surface atoms, we show regions (black triangles) where sections of (111) planes meet at a line which we designate as a "twin line," which strongly suggests that it is a precursor to the twin plane of an icosahedral structure. In Figs. 7(c) and 7(d), one can observe the formation of a twin plane, indicated by an arrow, directly below the twin line at the surface.

This illustrates once more that the initiation of ordering is at the surface even for the formation of the twinning planes.

Finally, to give a more complete picture of the evolution of these twinning planes after their initiation at the surface, we show the evolution with temperature of the hcp twin planes formed during quenching in Fig. 8. Figure 8 (left) shows the evolution as a function of temperature of both blocks of fcc order separated by hcp twinning planes. Also shown on the right at each time are the twinning planes themselves with the fcc blocks removed so that the evolution of these planes may be clearly seen. These show quite clearly that as the temperature is decreased, the overall particle evolves toward a nearly perfect icosahedral structure consisting of fcc fragments separated by hcp twinning planes. It also indicates that even at 298 K, imperfections exist in the as-grown structures, which is why the percentage of hcp ordered atoms indicated in Fig. 2 is slightly lower than that of a perfect icosahedron.

IV. CONCLUSIONS

The degree of crystallization of a liquid droplet of 10 179 atom gold nanoparticle quenched from the melt down to a range of temperatures from 1100 to 298 K was followed by use of $Q6$ order parameter and ring statistics. Structural ordering on the surface of the particle was easily observed by analysis of the formation of (111) planes characteristic of the surface of an icosahedral particle to which this particle evolved. However, analyzing the structural changes occurring in the core required an analysis based on planar graphs.[10]

We found that crystallization of the surface precedes that of the core, and the (111) region of the surface provides a template for the ordering of the core region.

A clear picture of the evolution as a function of temperature of the fcc blocks and hcp twinning planes characteristic of an icosahedral nanoparticle is also given.

ACKNOWLEDGMENTS

This project was supported by the Australian Partnership for Advanced Computing (APAC) and the Victorian Partnership for Advanced Computing (VPAC). One of the authors (Y.H.C.) would also like to thank RMIT University for its financial assistance.

*Corresponding author; salvy.russo@rmit.edu.au

[1] M. C. Danial and D. Astruc, Chem. Rev. (Washington, D.C.) **104**, 293 (2004); Y. Xiao, F. Patolsky, E. Katz, J. F. Hainfeld, and I. Willner, Science **299**, 1877 (2003).

[2] J. Pérez-Juste, I. Pastoriza-Santos, L. M. Liz-Marzán, and P. Mulvaney, Coord. Chem. Rev. **249**, 1870 (2005).

[3] T. K. Sau and C. J. Murphy, J. Am. Chem. Soc. **126**, 8648 (2004).

[4] J. Hu, Y. Zhang, B. Liu, J. Liu, H. Zhou, Y. Xu, Y. Jiang, Z. Yang, and Z.-Q. Tian, J. Am. Chem. Soc. **126**, 9470 (2004).

[5] M. A. Sanchez-Castillo, C. Couto, W. B. Kim, and J. A. Dumesic, Angew. Chem., Int. Ed. **43**, 1140 (2004).

[6] E. Hao, R. C. Bailey, G. C. Schatz, J. T. Hupp, and S. Li., Nano Lett. **4**, 327 (2004).

[7] K. Koga and K. Sugawara, Surf. Sci. **529**, 23 (2003); K. Koga, T. Ikeshoji, and K. Sugawara, Phys. Rev. Lett. **92**, 115507 (2004).

[8] H. S. Nam, N. M. Hwang, B. D. Yu, D. Y. Kim, and J. K. Yoon, Phys. Rev. B **71**, 233401 (2005).

[9] H. S. Nam, N. M. Hwang, B. D. Yu, and J. K. Yoon, Phys. Rev. Lett. **89**, 275502 (2002).

[10] Y. H. Chui, R. J. Rees, I. K. Snook B. O'Malley, and S. P. Russo, J. Chem. Phys. **125**, 114703 (2006).

[11] P. W. Sutter and E. A. Sutter, Nat. Mater. **6**, 363 (2007).

[12] B. O'Malley and I. K. Snook, Phys. Rev. Lett. **90**, 085702 (2003).

[13] P. R. ten Wolde, M. J. Ruiz-Montero, and D. Frenkel, Phys. Rev. Lett. **75**, 2714 (1995).

[14] F. Ercolessi, E. Tosatti, and M. Parrinello, Phys. Rev. Lett. **57**, 719 (1986).

[15] Available at http://www.pas.rochester.edu/~wangyt/algorithms/index.html

[16] J. D. Bernal, Nature (London) **183**, 141 (1959).

[17] D. S. Fransblau, Phys. Rev. B **44**, 4925 (1991).

[18] B. O'Malley and I. Snook, J. Chem. Phys. **123**, 054511 (2005).